Hindawi
Advances in Civil Engineering
Volume 2020, Article ID 7564684, 21 pages
https://doi.org/10.1155/2020/7564684

Research Article

Damage-Based Seismic Retrofitting Approach for Nonductile Reinforced Concrete Structures Using FRP Composite Wraps

Vui Van Cao and Son Quang Pham

Faculty of Civil Engineering, Ho Chi Minh City University of Technology (HCMUT)–Vietnam National University, 268 Ly Thuong Kiet Street, District 10, Ho Chi Minh, Vietnam

Correspondence should be addressed to Vui Van Cao; cvvui@hcmut.edu.vn

Received 4 November 2019; Revised 16 March 2020; Accepted 16 May 2020; Published 30 May 2020

Academic Editor: Filippo Ubertini

Applying similar amount of fibre reinforced polymer (FRP) for all plastic hinge locations in a structure is not an ideal approach as damage occurring at these critical locations may vary considerably. Building owners also always want to keep FRP retrofitting cost and associated interruption to a minimum. In this context, the current paper proposes an FRP retrofitting approach, in which FRP is selectively distributed based on the distribution of seismic damage in structures. The proposed approach, characterized by both quantitative and qualitative criteria, is simple but very effective in simultaneously reducing the seismic damage, amount of FRP to be used, and time of installation. For the considered cases of low- and mid-rise nonductile building structures, the FRP amount reduced approximately by 31% compared to the cases in which FRP was evenly distributed, leading to lower installation cost and less interruption time. Interestingly, although 31% FRP was saved, the damage indices of the FRP retrofitted frames were significantly lower than those in cases of even FRP distribution because FRP effectively served for critical locations. Due to its simplicity and technical/economical effectiveness, the proposed FRP retrofitting approach can be useful for engineering practice.

1. Introduction

Many existing reinforced concrete (RC) building structures around the world designed and built based on old codes have been identified to be deficient compared with current seismic codes [1]. One of the common deficiencies is of stirrups, leading to nonductile behaviour and low lateral load resistance of structures [1, 2]. Consequently, the weak beam-strong column mechanism is not achieved, and severe damage or collapse of buildings have been evident in the past earthquake events [1, 3]. Thus, mitigating the seismic risk by retrofitting these structures to meet the requirement of current seismic provisions, instead of demolishing and rebuilding, has been a solution of choice because of economic and social reasons. Extensive research has been devoted to the investigations of fibre reinforced polymer (FRP) applications in the past few decades, and FRP has been widely recognized as an economical engineering solution for retrofitting RC structures. Compared with conventional methods such as steel brace system, cross section enlargement or steel jacketing, FRP retrofit does not change the architecture or occupy the living space of buildings. In addition, FRP retrofit is much easier and quicker to install while FRP imposes almost no additional load on structures due to its lightweight. The high tensile strength and high corrosive resistance are also good characteristics, making FRP become the material of choice to retrofit beams [4–10], columns [11–16], joints [17–21], and structures [22–24].

FRP retrofitting aims at increasing the ductility, strength, and/or stiffness of existing structures. For structures with deficiency of transverse reinforcement, increasing the ductility should be taken as priority. FRP wraps provide confinement conditions which significantly increase the compressive strength and ultimate strain for concrete [25–28]. Consequently, the strength [29, 30], ductility [29, 30], and energy absorption capacity [29, 31] of columns retrofitted by FRP wraps greatly improved. Studies on minimizing the amount of FRP and thus the cost for

retrofitting of columns were also conducted by researchers [32, 33]. For frame structures, similar beneficial effects of FRP retrofitting have been confirmed by researchers. FRP retrofitting successfully prevented soft storey [1] and column-sway [34] mechanisms for structures. FRP retrofitting significantly increased the seismic capacity [3, 35–38] and considerably improved deformation capacity [34, 37], but reduced damage [34, 37, 39] for structures.

The above studies on FRP retrofitting of RC frames confirmed the effectiveness of FRP confinement applied to critical locations of plastic hinges to improve the seismic performance of RC structures; however, less attention has been paid for the cost of FRP retrofitting. Along with reducing to a predefined damage level for structures, the least amount of FRP and the shortest FRP installation time, to minimize the cost, are of major concerns by not only building owners but also structural/retrofitting engineers. Obviously, these concerns are not appropriately addressed by evenly distributing FRP for critical locations of plastic hinges because the seismic damage is unevenly distributed to these locations. To the best of the authors' knowledge, the number of studies aiming at addressing these concerns is quite limited in the literature as reviewed in the following. Thermou et al. [40] developed a methodology for upgrading deficient RC buildings, in which the distribution of the inter-storey drift is optimized by intervening the stiffness distribution in the vertical direction of the building. Zou et al. [41] optimized the performance-based design of FRP confinement at plastic hinges of columns for seismic retrofitting of existing RC structures. The optimization objective was to minimize the thickness of FRP confinement while the optimization process was subjected to the criterion of inelastic inter-storey drift. Choi et al. [42] proposed a seismic retrofitting method for shear-critical RC frames using FRP wraps with multiobjectives. The two objective functions were to minimize the amount of FRP and variation coefficient of the inter-storey drift while the constraint functions were the allowable inter-storey drift, the shear failure, and the maximum compressive strength of concrete. The optimal method was illustrated by the retrofitting of a three-storey frame.

Only limited number of studies [40–42] in which inter-storey drift was employed as the main criterion to distribute FRP, together with no clear guidelines in current codes applied for FRP distribution in frames, have inspired the authors to carry out this study. An attempt aiming at helping engineers to address the practical concern of FRP retrofitting cost raise by building owners and to improve the effectiveness of the FRP retrofitting is presented in this paper. To achieve this aim, an FRP retrofitting approach of RC structures, in which FRP is distributed based on the seismic damage distribution (instead of inter-storey drift) in structures, was proposed. Because the damage indices of plastic hinges (element damage level) are more specific than inter-storey drifts (storey damage level), the distribution of FRP based on damage indices is logically more appropriate. The technical and economical effectiveness proposed approach was demonstrated for the two FRP retrofitting cases of 4- and 8-storey nonductile RC frames representing for low- and mid-rise building structures. The frames were retrofitted by the proposed approach and then by evenly distributing the FRP for comparison. Conclusions are made based on the comparison.

2. The Proposed Damage-Based FRP Retrofitting Approach

Figure 1 shows the proposed FRP retrofitting approach for existing structures based on seismic damage distribution. Based on the design of a structure, the seismic damage distribution in structures is analysed. The obtained damage distribution is used to distribute the FRP. In this proposed FRP retrofitting approach, FRP is only applied to the locations of plastic hinges where the damage indices (DI) are larger than the allowable damage index [DI] while the locations with no or minor damage are not applied by FRP. This step is simple but very effective in appropriately distributing FRP. Two criteria are applied in the proposed retrofitting approach. The first criterion is quantitatively set by the condition DI $\leq$ [DI] while the second criterion is qualitatively set by the damage distribution. The proposed FRP retrofitting approach is described in Figure 1, followed by the general descriptions of steps. Some steps with long details are described in Sections 3 and 4. It is worth emphasizing that the details of long steps presented in these sections are of several methods that can be used. For example, the selection of seismic records can be different based on the seismic design codes, or the analysis method can be different provided the target is achieved:

(i) Step 1: existing structures

The design of building structures is collected, providing information for analyses and FRP retrofitting.

(ii) Step 2: design earthquakes and the allowable damage index [DI]

The design earthquake intensity is based on the current seismic code for the region where the retrofitted building is located. The characteristics of earthquakes occurring in the region are also collected if applicable. The design response spectrum regulated in current seismic codes for the region is constructed and earthquake ground motions are then selected. These selected ground motions are scaled to match the design response spectrum in order to obtain the scaled seismic records which are then used for inelastic time history (ITH) analyses.

The other task of this step is to determine the damage level for the retrofitted structures such as light damage, moderate damage, or severe damage when the retrofitted structure experiences the design earthquakes. The target damage level is established by the owners, managers, or investors under being consulted by structural engineers with a reference to current seismic codes. The target damage level is then used to determine the allowable damage index [DI]. This [DI] is used as a

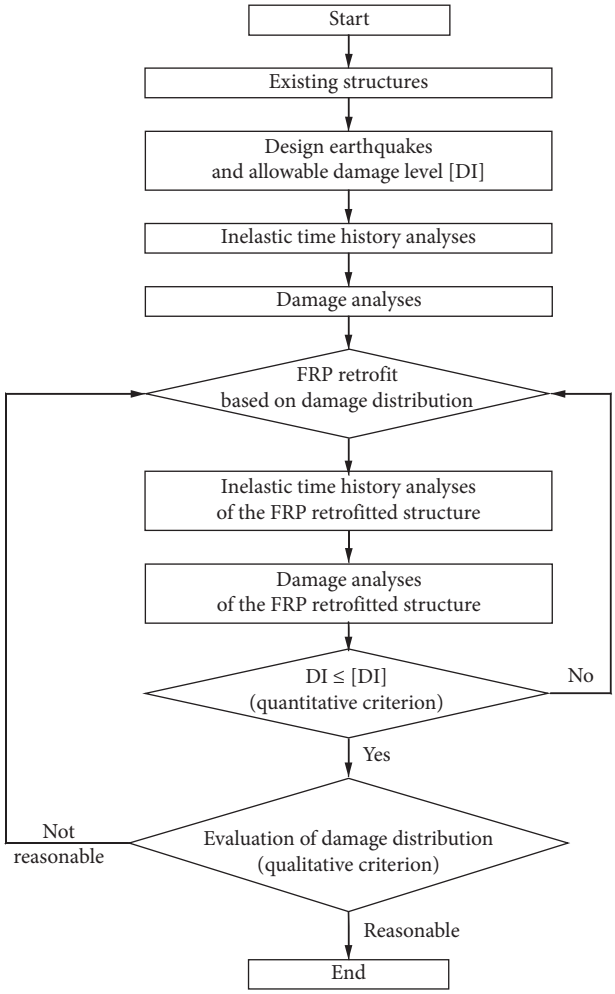

Figure 1: The proposed damage-based FRP retrofitting approach.

quantitative control criterion for the FRP retrofitting design, followed by the qualitative criterion of damage distribution.

(iii) Step 3: ITH analyses of RC frame

The structure is modelled for ITH analyses. These ITH analyses are performed for the structure subjected to the selected ground motions corresponding to the design seismic intensity established in Step 2. The details of ITH analyses are presented in Section 3.1.

(iv) Step 4: damage analyses

The results of hysteretic behaviours of plastic hinges obtained from ITH analyses in step 3 are exported in the form of Excel data files. Then, these data served for damage analyses conducted in MATLAB [43], expressed by damage indices. The obtained damage indices are then used to plot the damage distribution in structures. The details of damage analyses are presented in Section 3.2.

(v) Step 5: FRP retrofit based on damage distribution

Due to the deficiency of internal confinement, FRP wraps are applied to the plastic hinge locations to provide external confinement. The design of FRP confinement is presented in Section 4.1. The damage distribution in the frame is then used to distribute the FRP in a manner that one or two FRP plies are applied for severe damage locations where the damage indices are larger than the allowable damage index [DI]. No FRP is applied for the locations with no or minor damage. This simple FRP distribution directly aims at severe and moderate damage locations, making the retrofitting approach become more effective.

(vi) Step 6: ITH analyses of the FRP retrofitted frame

This step is similar to Step 3; however, the FRP confinement is included. The analyses for properties of FRP-confined RC plastic hinges are presented in Section 4.2 while ITH analyses of the FRP retrofitted frames are presented in Section 3.1.

(vii) Step 7: damage analyses of the FRP retrofitted frames

Similar to Step 4, the hysteretic behaviours of plastic hinges are exported in the form of Excel data files, which are then processed in MATLAB [43], and the damage of plastic hinges is quantified by the damage index. The damage indices are plotted to obtain the damage distribution in the frame. Evaluation of damage distribution is carried out to provide information for FRP redistribution and adjustment in the frame. The details of damage analyses are presented in Section 3.2.

(viii) Step 8: check the quantitative condition $DI \leq [DI]$ (quantitative criterion)

The quantitative condition $DI \leq [DI]$ is checked for all plastic hinge locations. If there are plastic hinge locations whose damage indices are not satisfied this condition, the FRP retrofitting for those locations is redesigned by applying one additional FRP ply; thus, go back to Step 5. Otherwise, go to Step 9.

For special situations of finance, the redesign should aim at not only at the locations whose damage index is larger than the allowable damage index but also the locations whose damage indices are too small. A simple rule can be applied: decrease one ply for plastic hinge where the damage index is much smaller than the [DI] and increase one ply for plastic hinges where $DI > [DI]$.

(ix) Step 9: evaluating the damage distribution (qualitative criterion)

When the quantitative condition $DI \leq [DI]$ is satisfied, the distribution of damage in the frame is qualitatively evaluated. This step is conducted based on the importance of storeys and elements. For example, the storey i is more important than storey i^+ (the above storeys) while it is less important than the storey i^- (the below storeys). The lowest storey can be the most important while the

top storey is the least important. Within a storey, columns should be more important than beams. Ideally, the damage index of the storey one is smallest and the damage index of the top storey is largest.

3. ITH and Damage Analyses

3.1. ITH Analyses. Under earthquake excitations, inelastic deformation is often developed at the critical regions of plastic hinges. The lump plasticity technique was employed for nonlinear modelling in this study. The details of the modelling were described in [22]; thus, only brief description is presented herein for convenience to readers. Linear and nonlinear elements were employed for the modelling. The nonlinear elements were used to capture the nonlinear and hysteretic behaviours of plastic hinges. The locations of nonlinear elements are at the centers of plastic hinges of beams and columns. Figure 2(a) shows the model of a four-storey three-bay frame. The locations of inelastic elements of beams are located at $(h_{\text{column}} + l_p^{\text{beam}})/2$, where, l_p^{beam} is the plastic hinge lengths of beams and h_{column} is the height of the column sections. Similarly, the locations of inelastic elements of columns are located at $(h_{\text{beam}} + l_p^{\text{column}})/2$, where, l_p^{column} is the plastic hinge lengths of columns and h_{beam} is the height of the beam sections.

The inelastic behaviours of plastic hinges are captured using a hysteretic model. Several hysteretic models are available in the literature; however, majority of these models excludes the crack of concrete in tension zone while the Takeda hysteretic model [44] includes the concrete cracking. Thus, the Takeda model is selected for damage analyses in this paper because the crack of concrete can be considered as the onset of damage. Figure 2(b) shows the Takeda hysteretic model [44] developed based on the force-deformation curve including the crack point (D_{cr}, P_{cr}) and the yield point (D_y, P_y). Details of this model can be found elsewhere [44].

The properties of nonlinear elements are moment-rotation curves of plastic hinges. These moment-rotation curves are obtained using the moment-curvature curves and the plastic hinge lengths. In this paper, the simple model of plastic hinge length $l_p = h$ proposed by Sheikh and Khoury [45] is adopted while the moment-curvature curves are obtained using fibre model. In moment-curvature analyses using fibre model, the cross section is discretized into many fibres as shown in Figure 3(a) which are assumed to experience pure longitudinal deformation. The distribution of strain in a cross section is assumed to be linear as shown in Figure 3(b). The maximum compressive strain ε_m and the position of the neutral axis Z_n are used to determine the strain distribution in the section. Correspondingly, the curvature is computed as $\varphi = \varepsilon_m / Z_n$.

The position of neutral axis Z_n is found when the force equilibrium is attained. The force equilibrium is established based on the fibre forces which are the products of fibre stresses and the fibre cross-sectional areas, and the axial force N acting on the section. For each fibre, the strain at the fibre centroid is used to compute the fibre stress using the stress-strain behaviour of fibre material. Amongst several stress-strain models [46–52] proposed for concrete, Park et al.'s [52] model takes into account the enhancement of the maximum stress and the strain at maximum stress due to the confinement effects; thus, this model is used in this paper. Equations (1) and (2) show the relationship between the stress f_c and the strain ε_c of concrete. The parameters of the model are shown in equations (3)–(6), in which ρ_s is the ratio of the volume of transverse reinforcement to that of the concrete surrounded by the transverse reinforcement, f_c' (MPa) is the strength of concrete, b'' denotes the concrete core width measured to the outside of transverse reinforcement, s_h denotes the spacing of transverse reinforcement:

$$f_c = f_c'' \left[\frac{2\varepsilon_c}{\varepsilon_o} - \left(\frac{\varepsilon_c}{\varepsilon_o} \right)^2 \right] \quad \text{if } \varepsilon_c \le \varepsilon_o, \tag{1}$$

$$f_c = f_c'' \left[1 - Z\left(\varepsilon_c - \varepsilon_o \right) \right] \ge 0.2 f_c'' \quad \text{if } \varepsilon_c \ge \varepsilon_o, \tag{2}$$

$$f_c'' = K f_c', \tag{3}$$

$$\varepsilon_o = 0.002K, \tag{4}$$

$$Z = \frac{0.5}{\left(3 + 0.29 f_c'/145 f_c' - 1000 \right) + (3/4)\rho_s \sqrt{\left(b''/s_h \right)} - 0.002K}, \tag{5}$$

$$K = 1 + \frac{\rho_s f_{yh}}{f_c'}, \tag{6}$$

After the neutral axis Z_n is determined, the moment $M = \sum_{i=1}^{n_f} F_i d_i$ with respected to the sectional mid-height axis, in which d_i is the distance from the centroid of the fibre i to the sectional mid-height axis; F_i is the force of fibre i which is equal to the product of the stress and the area of that fibre; and n_f is the number of fibres. Moment-curvature analyses were carried out in Matlab [43] up to the ultimate as plotted in Figure 3(d). Then, the moment-curvature curves are converted to moment-rotation curves by multiplying the plastic hinge lengths.

3.2. Damage Analyses. The hysteretic behaviours of nonlinear elements obtained from ITH analyses are exported for damage analyses, using a damage model. Compared with noncumulative damage models, cumulative damage models are more appropriate for damage analyses of structures subjected to earthquake excitations because the duration, number of cycles, and frequency content of the ground motions play important roles in damaging structures. In addition, the magnitude of damage index should vary from 0 to 1. DI = 0 refers to the state of no damage while DI = 1 refers to the state of collapse. The damage model proposed by Cao et al. [53] shown in equation (7) satisfied the just-mentioned characteristics and is used in this paper:

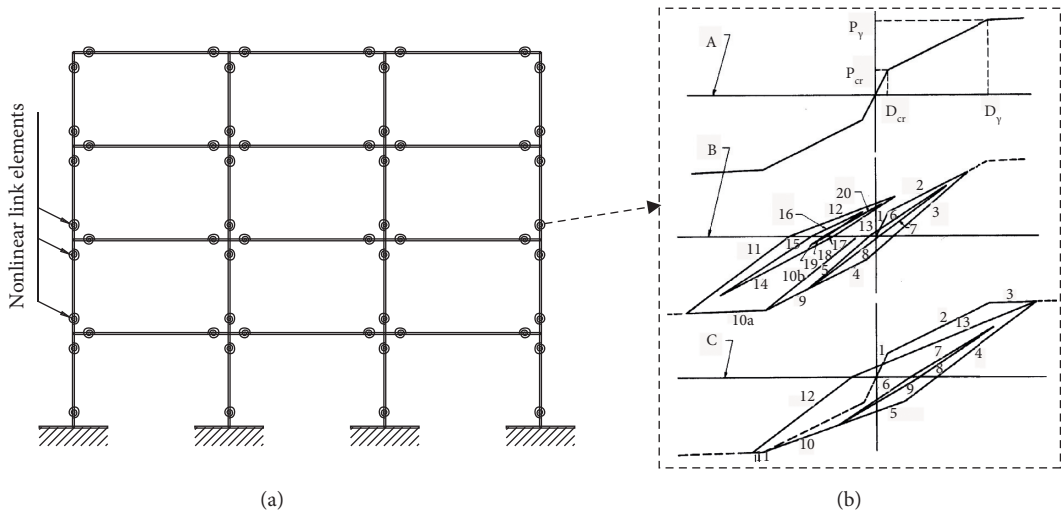

Figure 2: Modelling for inelastic analyses: (a) modelling and (b) hysteretic behaviour [44].

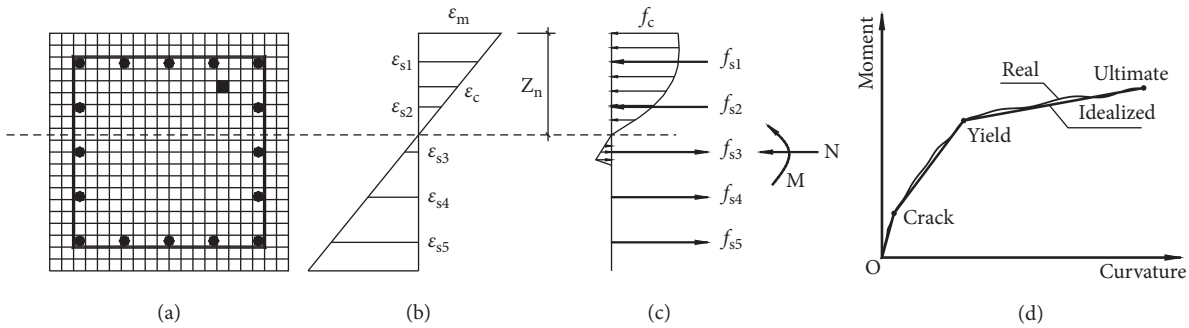

Figure 3: Section analysis using fibre model: (a) discretization, (b) strain, (c) stresses, and (d) moment-curvature.

$$\mathrm{DI} = \left[\frac{E_h}{E_h + E_{\mathrm{rec}}}\right]^{\alpha(N-i)}, \tag{7}$$

in which E_h is the cumulative hysteretic energy; E_{rec} is the cumulative recoverable energy; $N = E_{h,1\mathrm{collapse}}/E_{h,1y}$ is the equivalent number of yielding cycles to collapse; $i = E_h/E_{h,1y}$ is the equivalent number of yielding cycles at the current time of loading ($i \le N$); $E_{h,1\mathrm{collapse}}$ and $E_{h,1y}$ are, respectively, the hysteretic energy of one complete ultimate and one yielding cycle; and $\alpha = 0.06$ is a modification factor. Table 1 shows the damage levels with the legends corresponding to their damage indices and damage descriptions. The legends of damage are used to plot the damage states of frames in Sections 5–7.

Table 1: Damage levels.

Legend	Damage index	Description
.	0–0.05	No or minor
+	0.05–0.25	Light
x	0.25–0.50	Moderate
▲	0.50–0.75	Severe
●	0.75–1.00	Collapse

4. Design and Analyses of FRP Retrofitted Frames

4.1. Design of FRP Confinement. Providing external confinement using FRP wraps is an appropriate retrofitting solution applied to structures whose transverse steel inadequately confines the concrete. FRP wraps are applied to the plastic hinges of columns in the orientation of transverse reinforcement to confine concrete, leading to the enhancement of strength and ductility for concrete. The length of columns, on which FRP wraps are applied, is assumed to be twice the plastic hinge length l_p.

The effectiveness of FRP retrofitting depends on several factors such as the mechanical properties of FRP, the dimensions and shapes of cross sections, and the strength of unconfined concrete. For a given FRP type and the cross section, the total thickness of FRP is of importance in FRP retrofitting which governs the strength and ductility of FRP-confined concrete [41] as can be apparent in the Lam and Teng model [25, 54]. The thickness of one FRP ply is produced by manufacturers and is a constant. Therefore, the number of FRP plies is considered as a variable for the retrofitting design. In this study, the cost of FRP retrofitting is directly inferred from the amount of FRP. It should be

mentioned herein that the cost of FRP retrofitting also depends on the number of plastic hinges retrofitted by FRP due to the labour work and time of FRP installation. For example, with a similar amount of FRP, the retrofitting solution with fewer locations of FRP installation could be less labour work and shorter installation time; and such a solution is therefore cheaper.

The effectiveness of FRP wraps to improve the compressive strength and ductility of concrete has been widely confirmed in the literature. The tensile strength and modulus of GFRP are much lower than those of CFRP, providing larger displacement ductility for concrete; consequently, the aims of confinement and ductility improvement are better achieved by GFRP than CFRP as confirmed in [22, 55]. Additionally, GFRP is much cheaper than CFRP. Therefore, GFRP is used in this paper. The tensile strength and modulus of GFRP unidirectional fibre sheets provided by the manufacturers are 3241 MPa and 72397 MPa, respectively [56], while the thickness is 0.589 mm [56]. Figure 4 shows the design of GFRP wraps in which the plastic hinges of columns are wrapped by a number of GFRP plies. To avoid stress concentration leading to early failure of GFRP at corners, rounding corners of columns should be conducted before applying the GFRP wraps [57]. Rounding 50 mm at column corners [23, 41] is adopted in this study and is shown in Figure 4.

4.2. Inelastic Analyses of RC Frame Retrofitted by FRP Confinement. Because the FRP wraps is in the orientation of the transverse reinforcement, the strength and stiffness of FRP in the longitudinal direction of columns (axial axis of columns) can be neglected [41]. The effect of FRP wraps results in the improvement of stress-strain behaviour of concrete; thus, the moment-curvature analyses of sections confined by FRP are almost similar to moment-curvature analyses presented Section 3.1. The difference is that the stress-strain model of FRP-confined concrete is taken into account. The confinement effect of GFRP wraps increases the compressive strength and ultimate strain of concrete; thus, it has marginal effect on the plastic hinge locations of FRP-confined columns as proven in [29]. Therefore, the locations of plastic hinges in beams and columns of the retrofitted frame are unchanged compared with those of the original frame.

The stress-strain behaviour of FRP-confined concrete has been studied by many researchers [25, 26, 54, 58–60] and it is concluded that the strength and ductility of concrete increase significantly. Review on FRP-confined concrete models has been performed by Ozbakkaloglu et al. [61] for circular sections and Rocca et al. [62] for noncircular sections. Overall, the available models of FRP-confined concrete can be categorized into two types: with and without including the internal effect of transverse reinforcement. Both transverse reinforcement and FRP provides confinement for the concrete core surrounded by transverse reinforcement, while only FRP provides confinement to the cover concrete. The models of FRP-confined concrete simultaneously considering both confinement effects of FRP and transverse reinforcement are often complex due to the interaction between the internal and external confinements.

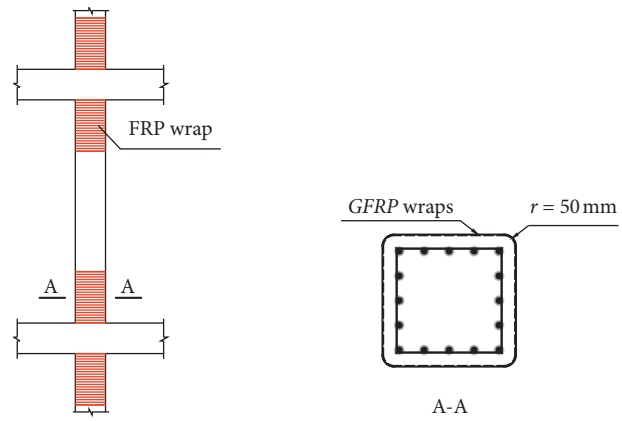

Figure 4: FRP wraps at locations of plastic hinges.

Additionally, the external confinement caused by FRP is much stronger than the poor internal confinement caused by the deficient transverse reinforcement. This stronger confinement of FRP can be proven by the fact that, after the strain 0.002 (approximately), the stress-strain branch of the FRP-confined concrete model ascends while that of the transverse-reinforcement confined concrete model descends. In addition, the purpose of FRP wraps is to provide additional confinement to poorly confined RC members. Therefore, for simplification, the poor internal confinement of transverse reinforcement is neglected in this study.

There are several stress-strain models [25, 54, 63–65] for concrete confined by FRP wraps available in the literature. Amongst these, Lam and Teng [25, 54] model is simple but adequately accurate and is adopted in ACI code [66]. In addition, this model was the most appropriate for circular and rectangular columns as proven by Rocca et al. [67] and has been used by many researchers [23, 55, 67]. Thus, the Lam and Teng [25, 54] stress-strain model for FRP-confined concrete is selected to use in this paper. Figure 5 illustrates the Lam and Teng [25, 54] model which includes two parts: the parabolic curve (branch OA) expressed by equation (8) and the linear branch (AB) expressed by equation (9). The parameters of the model are defined in equations (10)–(19):

$$\text{for } 0 \le \varepsilon_c \le \varepsilon_t : f_c = E_c\varepsilon_c - \frac{(E_c - E_2)^2}{4f_c'}\varepsilon_c^2, \tag{8}$$

$$\text{for } \varepsilon_t \le \varepsilon_c \le \varepsilon_u : f_c = f_c' + E_2\varepsilon_c, \tag{9}$$

in which

$$\varepsilon_t = \frac{2f_c'}{E_c - E_2}. \tag{10}$$

$$\frac{E_2 = f_{\text{cu}}' - f_c'}{\varepsilon_u}. \tag{11}$$

For rectangular columns, the ultimate stress f_{cu}' is computed using equation (12) or (13) and the ultimate strain ε_u is expressed by using equation (14). The parameters of these equations are described in equations (15)–(19), where

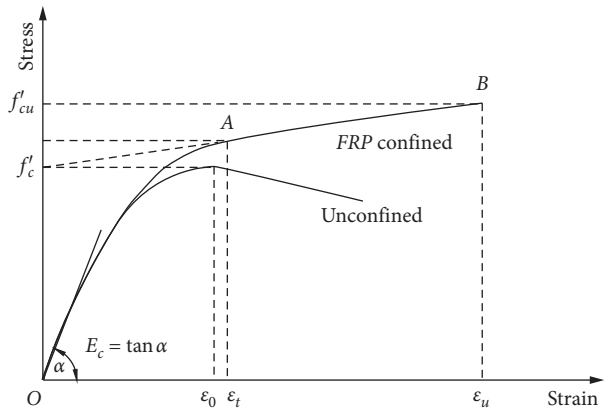

Figure 5: Stress-strain model of FRP-confined concrete proposed by Lam and Teng [25, 54].

t_f is the total thickness of FRP wraps, $\varepsilon_{h,\text{rup}}$ is the rupture strain of FRP, E_f is the modulus of FRP, and D is the equivalent diameter of circular column; k_{s1} and k_{s1} are shape factors described in equations (17) and (18), respectively, in which, b is the width and h is the depth of the cross section, r is the corner radius, and ρ_s is the ratio of longitudinal steel area to the cross sectional area:

$$f'_{\text{cu}} = f'_c\left[1 + 3.3k_{s1}\frac{f_{la}}{f'_c}\right], \quad if\ \frac{f_{la}}{f'_c} \geq 0.07, \tag{12}$$

$$f'_{\text{cu}} = f'_c, \quad if\ \frac{f_{la}}{f'_c} < 0.07, \tag{13}$$

$$\varepsilon_u = \varepsilon_o\left[1.75 + 12k_{s2}\frac{f_{la}}{f'_c}\left(\frac{\varepsilon_{h,\text{rup}}}{\varepsilon_o}\right)^{0.45}\right], \tag{14}$$

$$f_{la} = \frac{E_f t_f}{R}\varepsilon_{h,\text{rup}} = \frac{2E_f t_f}{D}\varepsilon_{h,\text{rup}}, \tag{15}$$

$$D = \sqrt{h^2 + b^2}, \tag{16}$$

$$k_{s1} = \left(\frac{b}{h}\right)^2\frac{A_e}{A_c}, \tag{17}$$

$$k_{s2} = \left(\frac{h}{b}\right)^{0.5}\frac{A_e}{A_c}, \tag{18}$$

$$\frac{A_e}{A_c} = \frac{1 - \left((b/h)(h-2r)^2 + (h/b)(b-2r)^2\right)/\left(3A_g\right) - \rho_s}{1-\rho_s}. \tag{19}$$

The rupture strain of FRP is defined as $\varepsilon_{h,\text{rup}} = k_\varepsilon\varepsilon_{frp}$, in which k_ε is the "strain efficiency factor" which is much smaller than 1. Researchers have proposed different values of k_ε for GFRP: 0.624 by Lam and Teng [25], 0.68 by Realfonzo and Napoli [68], and 0.66 by Baji et al. [69]. These values were of GFRP wraps for circular specimens subjected to monotonic axial compressive loading. In case of rectangular columns subjected to seismic loading, the value of k_ε should be smaller due to the higher stress concentration at corners and the effect of cyclic loading. Recently, Baji [70] analysed the test results of 184 GFRP-confined cylinder specimens subjected to axial loading and the average value 0.62 for k_ε is obtained. This smallest value of 0.62 which is close to the one proposed by Lam and Teng [25] was adopted in this paper.

5. Verifications

Verifications were conducted using different aspects of analyses: ITH analysis presented in Section 5.1, pushover analysis presented in Section 5.2, and damage analysis presented in Section 5.3.

5.1. Verification Using Time History Analysis. The analytical results of time history analyses were verified using the time history results of [34, 71] which were experimentally obtained from the shaking table tests of full-scale two-storey frame. The general view of the frame is shown in Figure 6(a) while the cross sections and the arrangement of steel are shown in Figure 6(b). Only brief descriptions are presented herein for convenience while the details can be found elsewhere [34, 71]. The vertical load for the shaking test included 45 kN of the steel plates attached to the floors and the self-weight of the frame and slabs. The compressive and tensile strengths of concrete were 20 MPa and 2 MPa, respectively, while its unit weight was 24 kN/m^3 and the elastic modulus was 25.5 GPa. The yield and ultimate strengths of steel were 551 MPa and 656 MPa, respectively, while the elastic modulus was 200 GPa. Steel ϕ6 mm and ϕ8mm were, respectively, used for stirrups of columns and beams.

The modelling technique described in Section 3 was employed to model the above full-scale tested frame using SAP2000 Version 19 software [72]. The periods of the first and second modes obtained from SAP2000 modal analysis are 0.54 s and 0.18 s which agree well with the experimental values 0.53 s and 0.18 s [34, 71]. The first and second mode shapes of the SAP2000 frame model are shown in Figure 7.

The SAP2000 [72] model of the frame was then subjected to seismic motions of the shaking table [34, 71] and time history nonlinear analyses were carried out. The history displacements of the first and second storeys obtained from analyses are compared with those obtained from the experiments, showing a good agreement as can be visible in Figure 8.

5.2. Verification Using Pushover Analysis. The 8-storey RC frame [55, 73] with its typical column and beam sections shown in Figure 9 is revisited for verification using pushover analysis. The dimensions are in mm; the steel is Grade 60 (f_y = 420 MPa); and the compressive strength of concrete was 25 MPa. The transverse reinforcement was Φ10 mm. The load on beams included 10 kN/m live load, 30 kN/m dead load, and the self-weight of the structure. The frame was designed based on UBC 1994 [74]; however, the spacing of transverse reinforcement is large, leading to nonductile behaviour of the frame, which needs to be retrofitted.

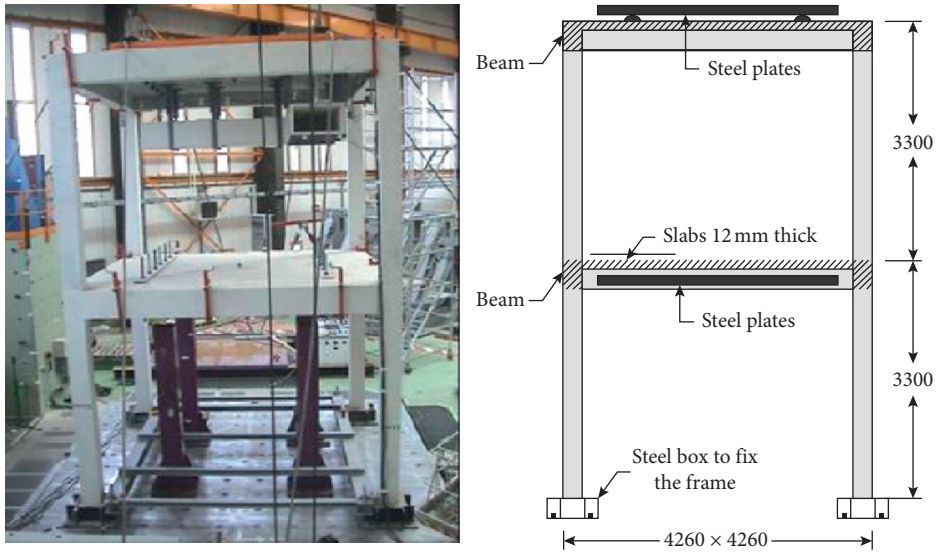

(a)

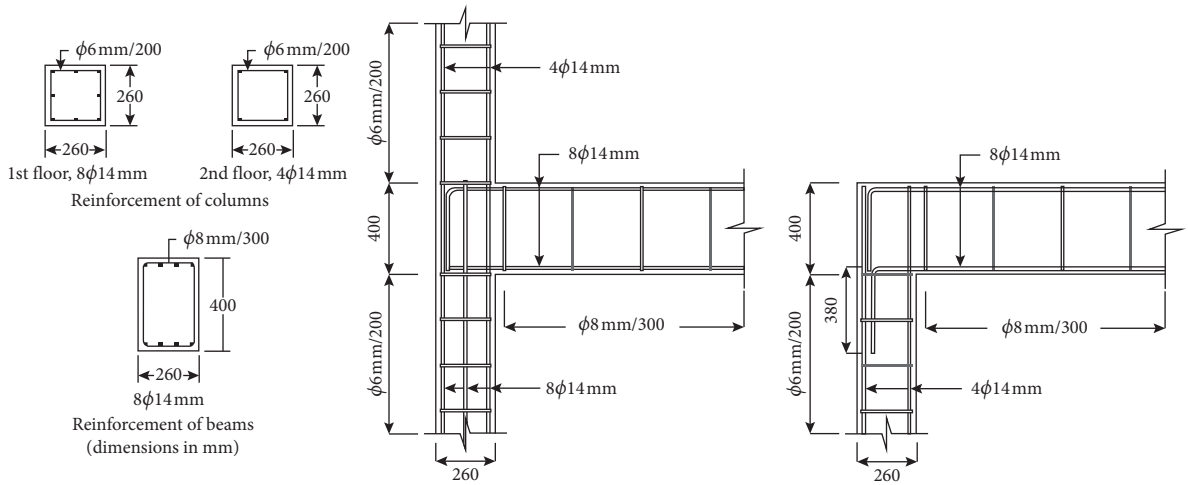

(b)

Figure 6: Full-scale 2-storey frame [34, 71]. (a) General view. (b) Cross sections and reinforcement arrangement.

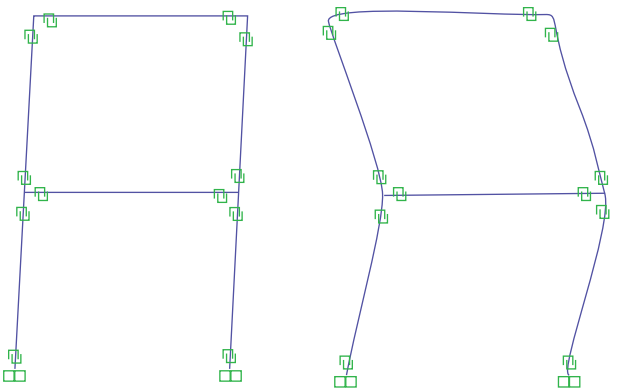

Figure 7: The first (left) and second mode shapes of the two-storey frame.

The frame under 100% dead load and 25% live load as recommended in many seismic codes was modelled in SAP2000 [72]. The fundamental period T was determined as 1.24 s, which agrees with the value 1.28 s analysed by Ronagh and Eslami [73]. Pushover analysis of the frame based on UBC code [74] is carried out. In this analysis, the equivalent lateral static seismic load F_i acting on each storey i and the additional force F_t acting on the top storey are computed using equations (20) and (21) [74], respectively, in which W_i is the seismic weight of storey i, h_i is the height of storey i, and V is the shear force. The analytical pushover curve compared with the curve analysed by Ronagh and Eslami [73] is shown in Figure 10, which indicates an overall approximation:

$$F_i = (V - F_t)\frac{W_i h_i}{\sum W_i h_i}, \tag{20}$$

$$F_t = 0.07TV \le 0.25V. \tag{21}$$

5.3. Verification Using Damage Mode. The tested three-storey RC building structure represented for buildings

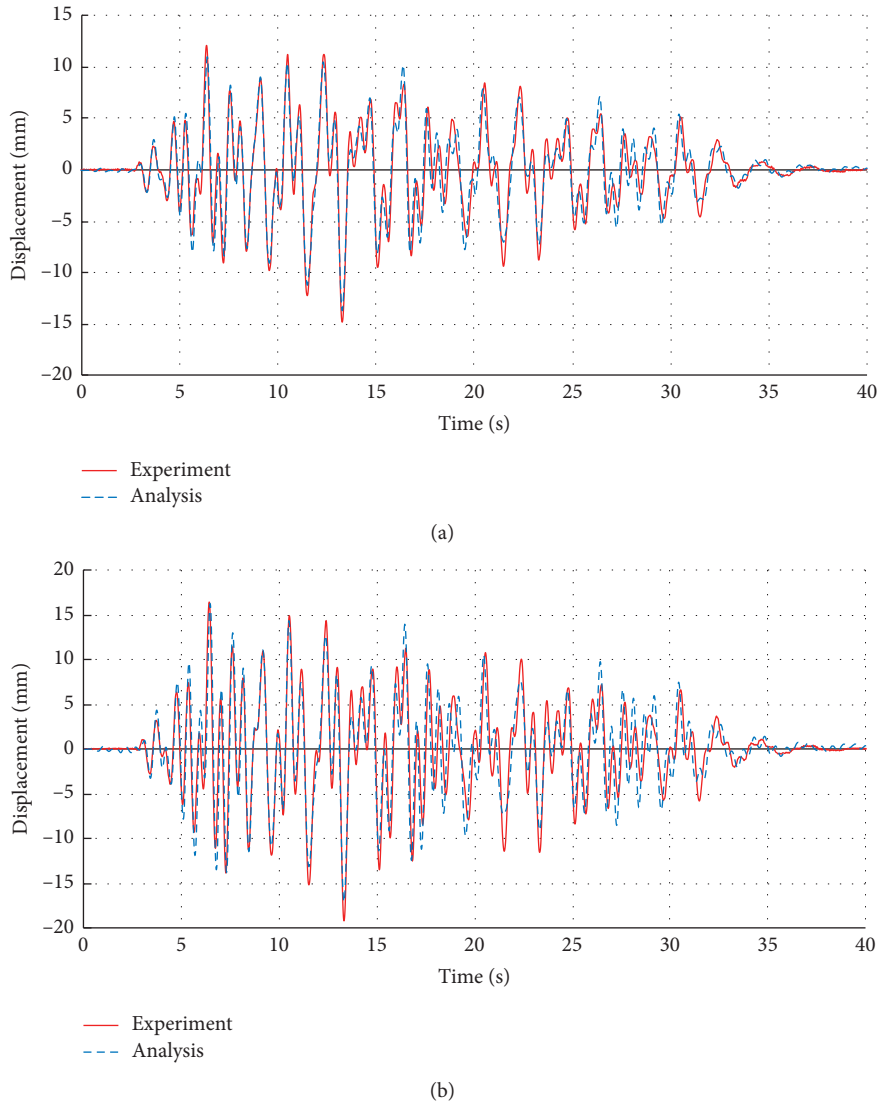

Figure 8: Comparison of the analytical and experimental [34, 71] history displacements. (a) Displacements of the 1st storey. (b) Displacements of the 2nd storey.

designed based only on gravity load shown in Figure 11 [75, 76] is used for verification of damage analysis. The average compressive strength of concrete f_c' was 27.2 MPa while its modulus was 24.2 GPa. The properties of steel are shown in Table 2. The total gravity load of each floor, which included the self-weight of the structure and the attached weights, was approximately 120 kN. More details can be found elsewhere [75, 76].

The frame was modelled in SAP2000 with the modelling details described in Section 3. The SAP2000 model was then subjected to the N21 E component with PGA = 0.20g of the Taft earthquake occurring on 21 July 1952 at the Lincoln School Tunnel site, California, which was used in the table shaking experiment. The hysteretic behaviours of nonlinear elements were then exported to MATLAB [43] to compute damage indices using Cao et al. [53] damage model. The damage indices were then used to plot the damage modes of the frame to compare with the experimental damage states. The legends shown in Table 1 are used to read the analytical damage levels shown in Figure 12. The comparisons presented in Figure 12 show overall agreements between the analytical and experimental damage states.

6. Case Study 1: Four-Storey RC Frame

(i) Step 1: existing structure

The 4-storey frame shown in Figure 13 [23] is used as a case study to demonstrate the proposed FRP retrofitting approach. The dead load included the distributed load 30 kN/m on beams and the self-weight of the frame while the live load was 10 kN/m. The tensile strength of steel f_y was 420 MPa and the compressive strength of concrete f_c' was 25 MPa. The modulus of concrete $E_c = 4700\sqrt{f_c'}$ [78] is adopted. Steel Φ10 mm was used for stirrups. The frame was located in seismic zone 3 and

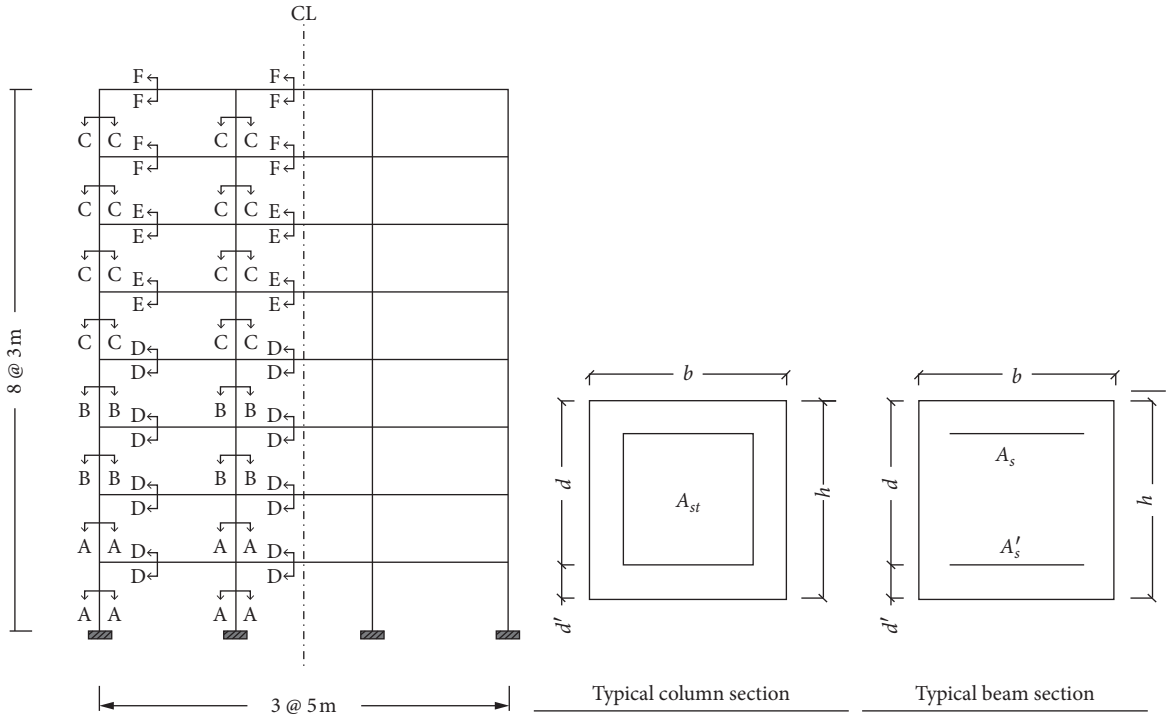

Section	b	h	d	d'	A_{st}	A_s	A'_s	Shear steel spacing (mm)
A-A	600	600	540	60	16ϕ25	-	-	450
B-B	600	600	540	60	16ϕ18	-	-	450
C-C	600	600	440	60	16ϕ16	-	-	450
D-D	600	600	440	60	-	6ϕ25	4ϕ25	140
E-E	600	600	440	60	-	6ϕ22	4ϕ22	175
F-F	600	600	440	60	-	6ϕ18	3ϕ18	250

Figure 9: Eight-storey frame [55, 73].

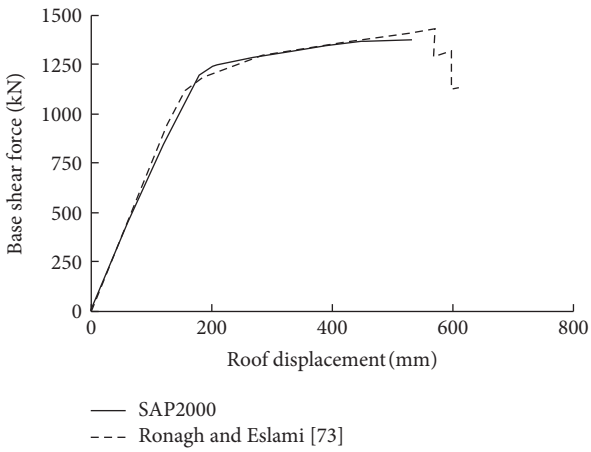

Figure 10: Comparison of pushover curves.

was designed in accordance with UBC 1994 [74]; however, the large spacing of stirrups leads to nonductile behaviour of the frame and the need of retrofitting. More details of the design can be found in [23].

(ii) Step 2: design earthquake ground motions and allowable damage index [DI]

The building is assumed to be located in the seismic zone 3 based on UBC code [74]; thus, the seismic zone factor $Z = 0.3$ and the seismic coefficients $C_a = 0.36$ and $C_v = 0.54$ are determined based on UBC code [74]. This is a standard occupancy structure, of which the seismic important factor is 1 while the importance factor of the building is 8.5 [74]. The building is assumed to be located in stiff soil D which is similar to type D in FEMA code [79]. The building is not located in near-fault region; thus, near-source factors $N_a = 1$ and $N_v = 1$. The seismic source type is B with the earthquake magnitude larger than 6.5. The design response spectrum/PGA is established as shown in Figure 14.

The model was then analysed and the fundamental period (T) of the frame was determined as 0.764 s.

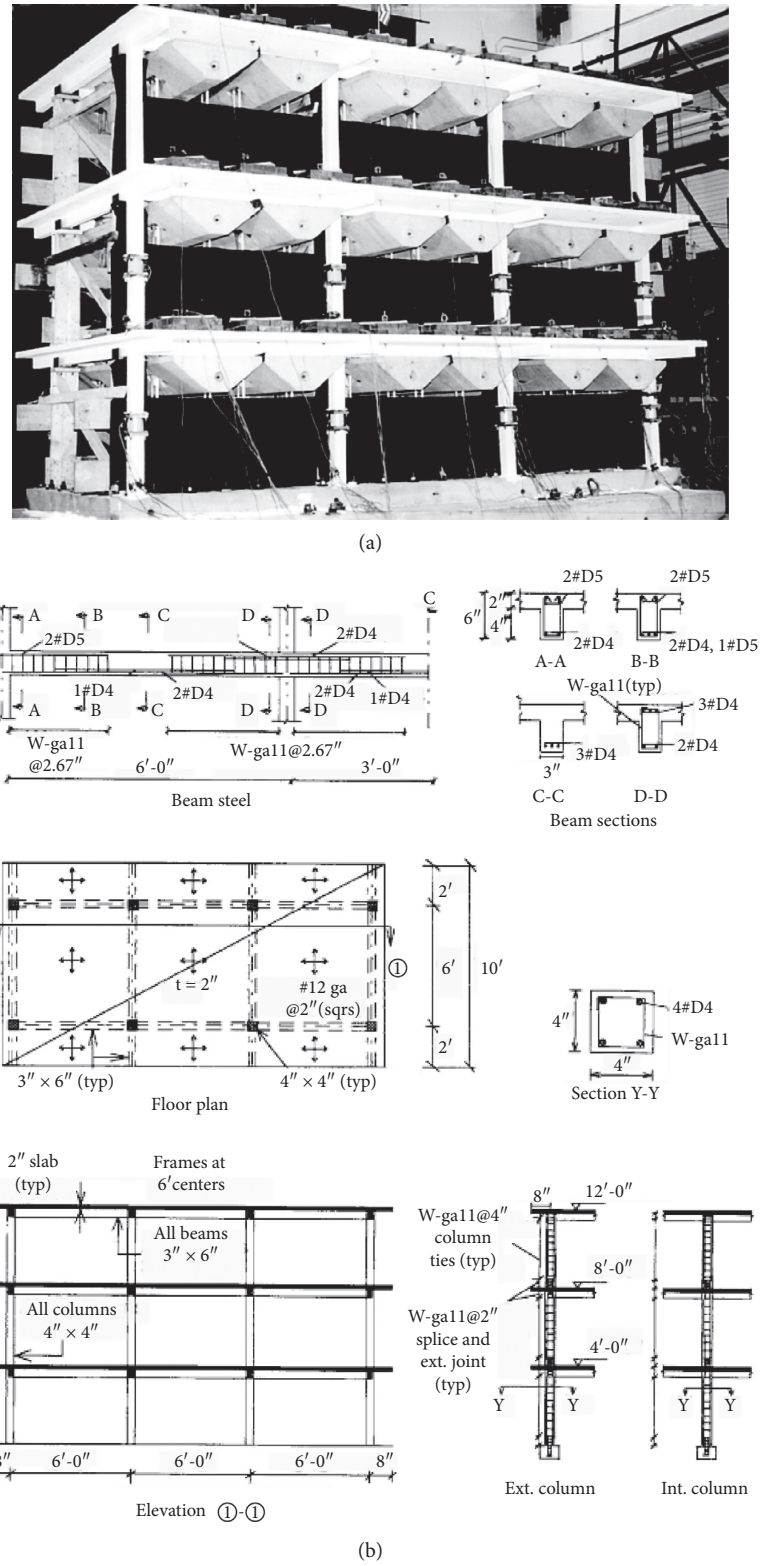

Figure 11: Three storey frame [75]. (a) General view. (b) Details (note: 1 in = 25.4 mm).

Seismic records are then selected and scaled to match the design response spectrum. The criterion for scaling the seismic records suggested by ASCE code [80] is adopted in this paper. Based on ASCE code [80], the mean value of the 5% damped response spectra of the selected scaled seismic records is not less than the target response spectrum over the range [0.2T-1.5T]. The scaling result using

Table 2: Steel properties.

Steel	Diameter (mm)	Yield strength (MPa)	Ultimate strength (MPa)	Modulus (MPa)	Ultimate strain
*D*4	5.715	468.86	503.34	214090	0.15
*D*5	6.401	262.01	372.33	214090	0.15
12 ga.	2.770	399.91	441.28	206161	0.13
11 ga.	3.048	386.12	482.65	205471	0.13

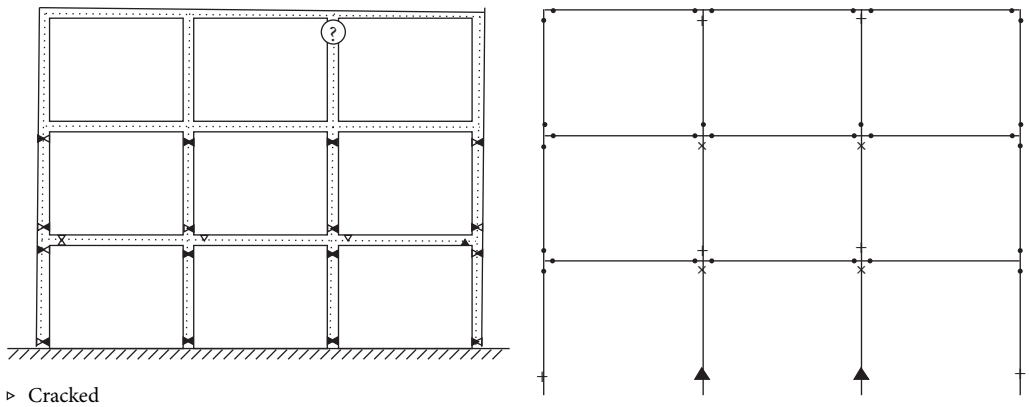

Figure 12: Comparison of damage modes. (a) Experiment [76] and (b) analysis.

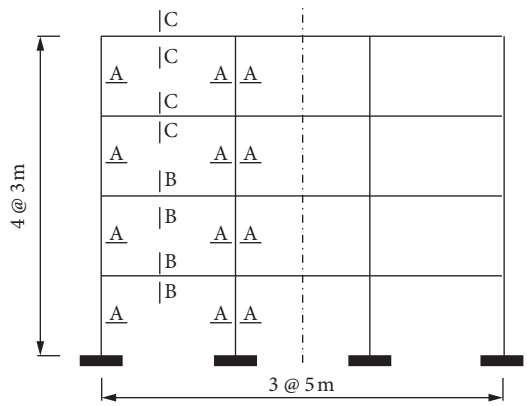

Section	b (mm)	h (mm)	d (mm)	d′ (mm)	A_{st} (mm^2)	A_s (mm^2)	A'_s (mm^2)	Spacing of stirrups (mm)
A-A	500	500	440	60	16ϕ18	-	-	450
B-B	500	500	440	60	-	6ϕ22	4ϕ22	175
C-C	500	500	440	60	-	6ϕ18	3ϕ18	250

Figure 13: Four-storey frame [23].

PEER database software [77] is shown in Figure 15. Two horizontal components of each earthquake station were used for the scaling as employed in the PEER database software [77]. Eight seismic records of four stations were selected, scaled, and used for analyses. The information and scale factors of these 8 seismic records are shown in Table 3, in which RSN is the record sequence number. As regulated in ASCE code [80], if the number of seismic records is equal or larger than 7, the average output

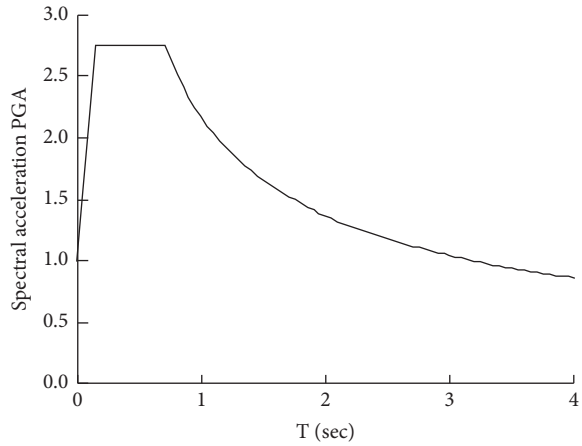

Figure 14: Spectral acceleration/PGA.

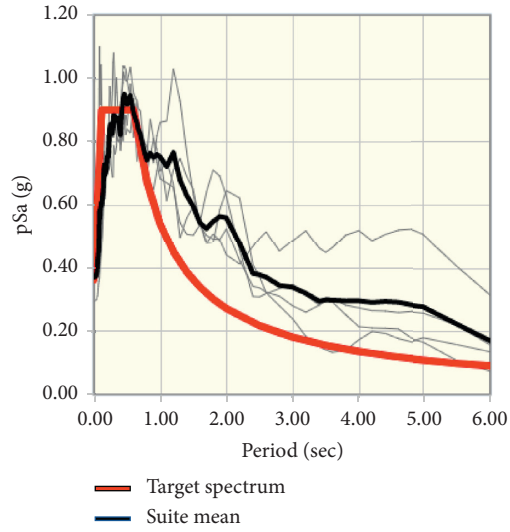

Figure 15: Scaling records to match the target spectrum [77].

Table 3: Selected records and scale factors.

Number	RSN	Scale factor	Event	Year	Station	Magnitude
1	861	6.440	Landers	1992	Barstow	7.28
2	859	7.265	Landers	1992	Hacienda Height-Colima	7.28
3	1215	5.822	Chi Chi, Taiwan	1999	CHY058	7.62
4	1488	3.303	Chi Chi, Taiwan	1999	TCU048	7.62

parameters are used; thus, the damage index of a plastic hinge is the average damage index of 8 damage indices.

In this case study, minor damage is assumed as the limit damage for the FRP retrofitted frame. To achieve this damage state, the allowable damage index [DI] is set as 0.25.

(iii) Step 3: ITH analyses

100% dead load and 25% live load are used for ITH analyses of the frame subjected to the selected ground motions. The moment-curvature analyses of sections and moment-rotation curves of plastic hinges were performed in MATLAB [43] using fibre model described in Section 3.1. The moment-rotation curves of plastic hinges were then assigned for the nonlinear elements in SAP2000 [72]. When the SAP2000 model of the frame was built, ITH analyses are conducted. The results from ITH analyses are then used for damage analyses in Step 4.

(iv) Step 4: damage analyses

The hysteretic moment-rotation behaviours obtained from the ITH analyses in Step 3 are exported to Excel and processed in MATLAB [43] to compute the demand parameters and damage indices using Cao et al. [53] damage model. The computation of damage index was applied for every nonlinear element of plastic hinges and for each ground motion. As a result, 56 damage indices of 56 plastic hinges were obtained when the frame subjected to a ground motion. The procedure was carried out for 8 ground motions of the design intensity; thus, each plastic hinge had 8 damage indices. For each plastic hinge, the average of these 8 damage indices was the damage index of that hinge. Consequently, the 56 average damage indices were obtained for the frame subjected to the design seismic intensity. These 56 average damage indices were then used to plot the damage distribution in the frame as shown in Figure 16(a). The damage mode in Figure 16(a) is used for damage evaluation, providing useful information for the adjustment of FRP distribution. It should be mentioned that, for comparison, the damage states of the frames retrofitted by the proposed approach (Figures 16(b) and 16(c)) and by even distribution of FRP (Figure 16(d)) are also plotted in the same figure. Details of these Figures 16(b)–16(d) are presented in the following steps.

(v) Step 5: retrofit of structures based on damage distribution

The damage distribution shown in Figure 16(a) provides a clear picture of damage mode which is useful to distribute the FRP correspondingly, in which the larger amount of FRP is saved for the locations with severe damage while no FRP is applied to the locations with no or minor damage. By observing the damage distribution in Figure 16(a), the two inner columns of the first storey suffered severe damage (▲) while the two outer columns of the first storey and the two inner columns of the second storey experienced light damage (+). Two FRP ply was applied to these locations. Other locations in the frame such as beams of all storeys and columns of the third and the fourth storey have minor damage (.); thus, FRP was not applied to these minor damage locations. This FRP retrofitted frame is called RS1 which stands for retrofitted structure in the first time using the proposed approach.

(vi) Step 6: ITH analyses of the retrofitted frames

After the frame was retrofitted in Step 5 using the proposed retrofitting approach, ITH analyses of this FRP retrofitted frame (RS1) subjected to the selected 8 ground motions were carried out. The analytical details of the retrofitted frame are presented in Section 3 with the inclusion of the FRP confinement.

(vii) Step 7: damage analyses of the retrofitted frames

The hysteretic behaviours of nonlinear elements obtained in Step 6 were then exported to Excel and processed in MATLAB [43] to compute damage indices. The damage mode of RS1 is plotted in Figure 16(b).

(viii) Step 8: evaluate the damage using the damage index criterion $DI \leq [DI]$.

The quantitative condition $DI \leq [DI]$ is checked for all plastic hinges of the RS1. All plastic hinge locations satisfy this condition, so go to Step 9.

(ix) Step 9: evaluate the damage distribution in the structure

When the quantitative criterion $DI \leq [DI]$ is satisfied for all plastic hinges, the qualitative criterion on the damage distribution in the frame is evaluated. The damage mode shown in Figure 16(b) is used to evaluate the damage distribution in the frame. For storey 1, the damage indices of the two inner columns are much larger than those of the two outer columns. The FRP adjustment can be made so that the damage indices of columns in the same storey should be similar. Ideally, the damage indices of the lower storeys should be less or equal than those of the higher storey because the lower storeys are more important than the higher storeys.

Additional redesign of FRP by adding one ply to plastic hinges at the bottom ends of the inner columns of the first storey is conducted. This FRP retrofitted structure is called RS2. The procedure is similar and the result is shown in Figure 16(c). The damage index decreases from 0.107 to 0.077.

For comparison, the frame retrofitted by even distribution of FRP was also carried out. One FRP ply was applied for all plastic hinges and this retrofitted frame is called RS0. The number 0 denotes that the frame is retrofitted without using the proposed retrofitting approach. ITH and damage analyses of this frame RS0 were performed and the damage state is plotted in Figure 16(d). Although all plastic hinges of the frame were applied by two FRP plies, the damage state of RS0 is worse than the damage states of RS1 and RS2.

For further comparison, the maximum damage index of each storey was used to plot the damage distribution of storeys. The storey damage distributions of the original, RS0, RS1, and RS2 are shown in Figure 17. The damage state of the frame using the proposed retrofitting approach is significantly improved, showing the technical effectiveness of the proposed approach.

The comparison in terms of retrofitting cost is also carried as follows. The amount of FRP used for the retrofitted frame RS0, RS1, and RS2 were computed and plotted in Figure 18. In order to plot the

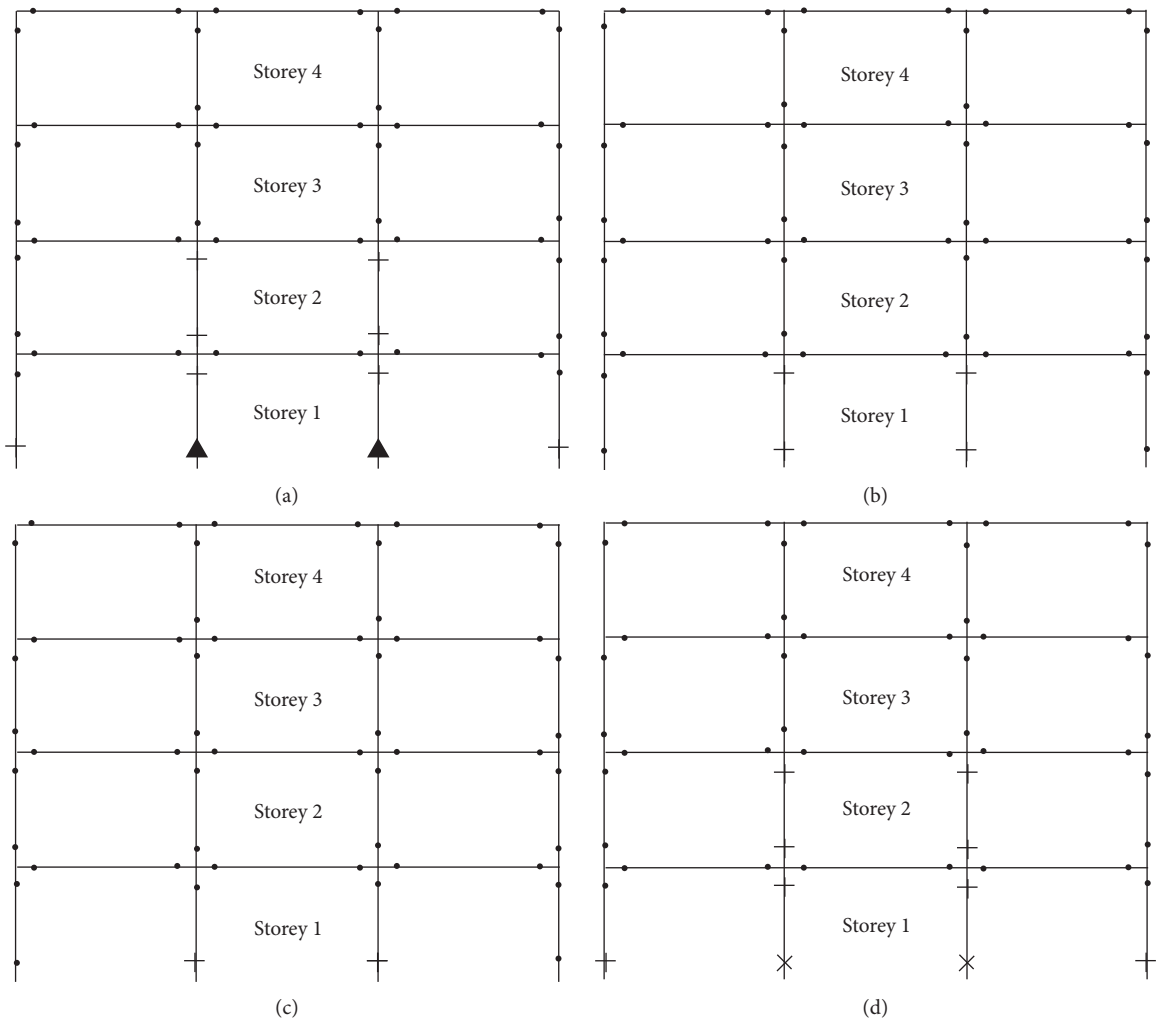

Figure 16: Damage distribution in frames. (a) Original, (b) RS1, (c) RS2, and (d) RS0.

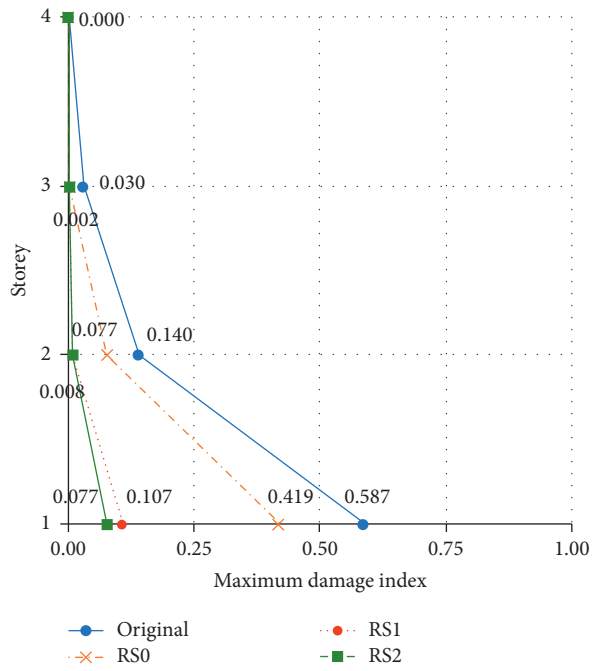

Figure 17: Distribution of storey damage of 4-storey frame.

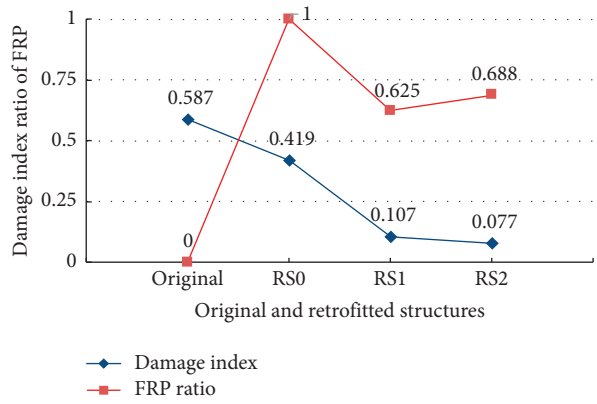

Figure 18: Variations of damage index and FRP ratio.

Table 4: Records and scale factor.

Number	RSN	Scale factor for intensity of	Event	Year	Station	Magnitude
1	1155	3.119	Kocaeli, Turkey	1999	Bursa Tofas	7.51
2	1604	21.851	Duzce, Turkey	1999	Cekmece	7.14
3	2095	20.320	Denali, Alaska	2002	Anchorage-DOI Off. of Aircraft	7.9
4	5824	15.521	El Mayor-Cucapah, Mexico	2010	CICESE	7.2

damage indices whose magnitudes vary from 0 to 1 and the amount of FRP of retrofitted frames RS0, RS1. and RS2 in the same figure (the same vertical axis) for visual comparison, the amount of FRP is normalized. The normalization is conducted by dividing the FRP amount by that of the RS0. Figure 18 shows that the original frame has a large damage index 0.587 which shows the severe damage of the original frame. With one ply applied for all plastic hinge locations, the damage index of RS0 decreases to 0.419. When the proposed FRP retrofitting approach is applied, the damage index and the amount of FRP significantly decrease. Particularly, the damage index decreases to 0.107 and the amount of FRP decreases 37.5% (decrease to 62.5%). With further adjustment of the FRP design (the frame RS2), the damage index further decreases and the FRP ratio slightly increases.

With the proposed FRP retrofitting approach, not only the amount of FRP but also the damage index reduces compared with the case of even distribution of FRP. Thus, the cost reduces and the retrofitting becomes more effective by reducing a larger amount of damage index. It is worth mentioning that, with the proposed retrofitting approach, several locations of plastic hinges are identified to be no or minor damage and thus FRP retrofitting is not needed. This is consequently helpful in shortening the FRP installation and interruption time, additionally reducing the retrofitting cost and bringing social benefit.

7. Case Study 2: 8-Storey Frame

The steps in this case study are similar to Case Study 1. Therefore, only the results and brief discussions are presented to avoid repeating the information of Case Study 1.

Steps 1–2: existing structures, the design earthquake ground motions, and the allowable damage index [DI]

The eight-storey frame described in Section 5.2 was used for Case Study 2. The ground motions were selected and scaled to match the design response spectrum. The building was assumed to be located in seismic region with PGA 0.30g. Table 4 shows the records of four earthquakes with the scale factor and the record sequence number (RSN).

Steps 3–4: ITH and damage analyses of the original frame

ITH and damage analyses were performed for the frame subjected to the selected ground motions. The damage distributions are shown in Figure 19(a).

Steps 5–8: retrofit of structures based on damage distribution, dynamic, and damage analyses

Steps 5–8 were carried out for the frames retrofitted by the proposed approach (RS1). The frame RS1 was retrofitted by applying 2 FRP plies to moderate damage locations (×) and one FRP ply was applied to locations with light damage (+). ITH and damage analyses of these frames were performed for the above frames. The damage state of the frame RS1 is shown in Figure 19(b).

Step 9: evaluate the damage distribution in the structure

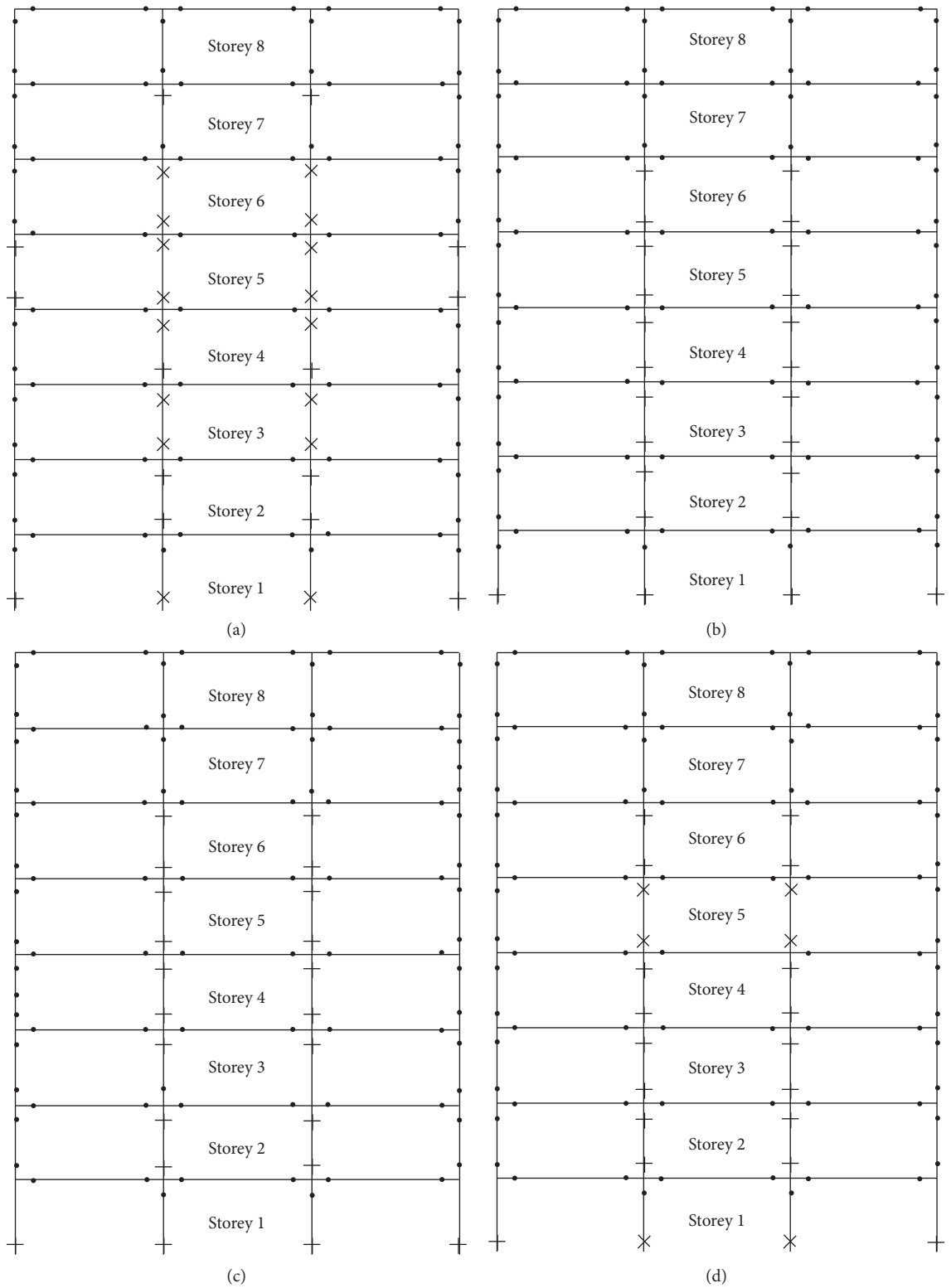

Figure 19: Damage of the 8-storey frame: (a) original, (b) RS1, (c) RS2, and (d) RS0.

Based on the damage distribution of the frame RS1 and the importance of lower storeys, the frame RS1 was retrofitted by adding 1 FRP ply to plastic hinges at the bottom ends of storey 1 inner columns and the plastic hinges of inner columns of storey 3, making the number of FRP plies, respectively, increase to 3 and 2 for these locations; and this frame is called RS2. The damage state of the frame RS2 is shown in Figure 19(c).

These analyses were also performed for the frame retrofitted by 1 FRP ply for all plastic hinges. This

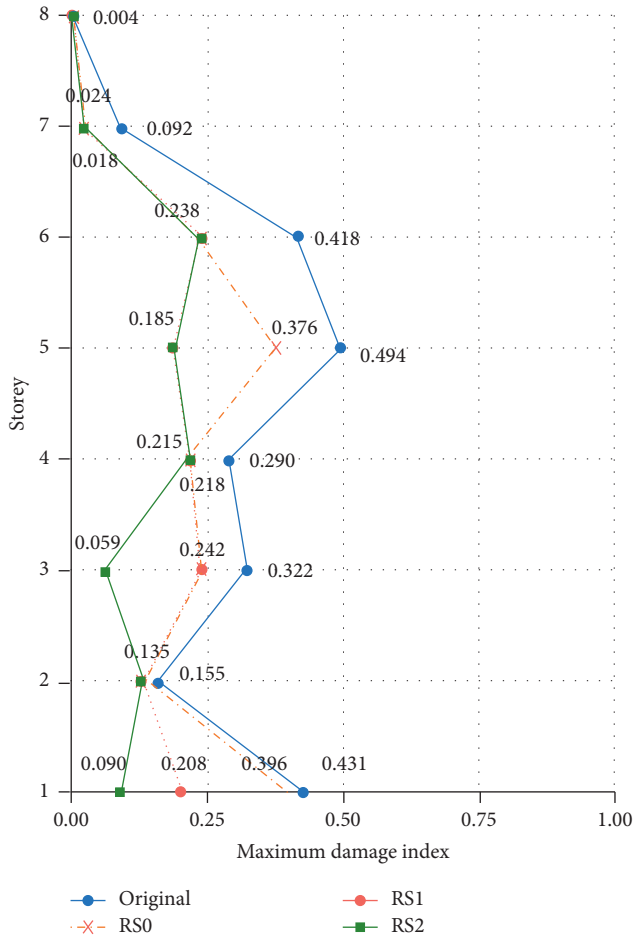

Figure 20: Distribution of storey damage of 8-storey frame.

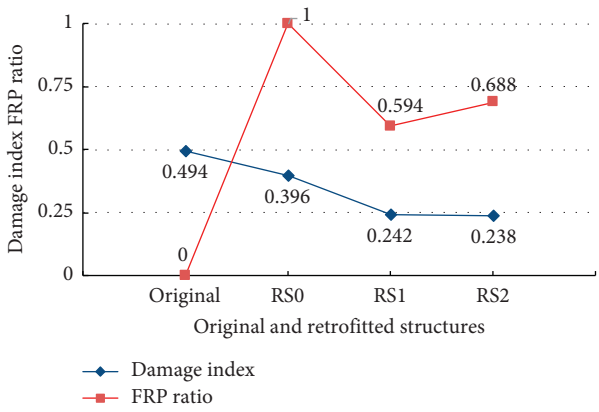

Figure 21: Variations of damage index and FRP ratio.

retrofitted frame is called RS0. The damage state of the retrofitted frame is shown in Figure 19(d). The distributions of storey damage indices of the original, RS0, RS1, and RS2 are plotted in Figure 20. Figure 21 shows the variations of damage index and the FRP ratios for the frames. As can be visible in Figures 20 and 21, of the frame RS2, the damage index is significantly reduced from 0.396 (moderate damage) to 0.238 (light damage) and the FRP ratio reduced to 68.8% when compared with that of the frame RS0. By coincidence, the value 68.8% is similar to the FRP ratio of the 4-storey frame.

8. Conclusions

This current paper presents the proposed FRP retrofitting approach to address building owners' concern on reducing the FRP cost and installation/interruption time. The FRP retrofitting approach is proposed based on the seismic damage distribution in structures, using both quantitative and qualitative criteria. The quantitative criterion is set by the condition $DI \leq [DI]$ and the qualitative criterion is evaluated by the damage distribution. The advantages of the proposed approach can be listed as follows: (1) the damage index and the damage mode of retrofitted structures are controlled; (2) the amount of FRP is reduced because FRP is effectively redistributed based on the damage distribution in structures; and (3) FRP installation/interruption time is reduced since only critical locations undergo retrofitting. The second advantage directly reduces the FRP material cost while the third advantage indirectly reduces the total retrofitting cost.

The proposed FRP retrofitting approach was used to retrofit low- and mid-rise nonductile RC frame structures. With a similar predefined target of damage level, the amount of FRP used for low- and mid-rise frames reduced to 68.8%. This resulted in 31.2% saving in FRP when compared with the traditional approach where FRP is evenly distributed. In addition, the damage indices of the considered low- and mid-rise FRP-retrofitted frames using the proposed retrofitting approach were much lower than those of the frames retrofitted using traditional approach. Thus, the proposed retrofitting approach not only reduced the cost but also was very effective in reducing the seismic damage. Due to its simplicity and technical/economical effectiveness, the proposed FRP retrofitting approach can be useful for engineering practice in retrofitting structures.

Data Availability

The data used to support the findings of this study are available from the corresponding author upon request.

Conflicts of Interest

The authors declare that they have no conflicts of interest.

Acknowledgments

This research was funded by Vietnam National Foundation for Science and Technology Development (NAFOSTED) under Grant no. 107.02–2017.18.

References

[1] J. Shin, D. W. Scott, L. K. Stewart, C.-S. Yang, T. R. Wright, and R. DesRoches, "Dynamic response of a full-scale reinforced concrete building frame retrofitted with FRP column jackets," *Engineering Structures*, vol. 125, pp. 244–253, 2016.

[2] P. Paultre and F. Légeron, "Confinement reinforcement design for reinforced concrete columns," *Journal of Structural Engineering*, vol. 134, no. 5, pp. 738–749, 2008.

[3] I. Erdem, U. Akyuz, U. Ersoy, and G. Ozcebe, "An experimental study on two different strengthening techniques for RC frames," *Engineering Structures*, vol. 28, no. 13, pp. 1843–1851, 2006.

[4] J. W. Schmidt, C. O. Christensen, P. Goltermann, and K. D. Hertz, "Shared CFRP activation anchoring method applied to NSMR strengthening of RC beams," *Composite Structures*, vol. 230, p. 111487, 2019.

[5] B. Fu, J. G. Teng, G. M. Chen, J. F. Chen, and Y. C. Guo, "Effect of load distribution on IC debonding in FRP-strengthened RC beams: full-scale experiments," *Composite Structures*, vol. 188, pp. 483–496, 2018.

[6] Y. Liu and Y. Fan, "Experimental study on flexural behavior of prestressed concrete beams reinforced by CFRP under chloride environment," *Advances in Civil Engineering*, vol. 2019, Article ID 2424518, 14 pages, 2019.

[7] A. M. H. Kadhim, H. A. Numan, and M. Özakça, "Flexural strengthening and rehabilitation of reinforced concrete beam using BFRP composites: finite element approach," *Advances in Civil Engineering*, vol. 2019, Article ID 4981750, 17 pages, 2019.

[8] N. Askandar and A. Mahmood, "Comparative investigation on torsional behaviour of RC beam strengthened with CFRP fabric wrapping and near-surface mounted (NSM) steel bar," *Advances in Civil Engineering*, vol. 2019, Article ID 9061703, 15 pages, 2019.

[9] N Basa, M. Ulicevic and R. Zejak, "Experimental research of continuous concrete beams with GFRP reinforcement," *Advances in Civil Engineering*, vol. 2018, Article ID 6532723, 16 pages, 2018.

[10] K. Chansawat, T. Potisuk, T. H. Miller, S. C. Yim, and D. I. Kachlakev, "FE models of GFRP and CFRP strengthening of reinforced concrete beams," *Advances in Civil Engineering*, vol. 2009, Article ID 152196, pp. 1–13, 2009.

[11] E. del Rey Castillo, M. Griffith, and J. Ingham, "Seismic behavior of RC columns flexurally strengthened with FRP sheets and FRP anchors," *Composite Structures*, vol. 203, pp. 382–395, 2018.

[12] J.-J. Zeng, Y.-C. Guo, W.-Y. Gao, W.-P. Chen, and L.-J. Li, "Stress-strain behavior of concrete in circular concrete columns partially wrapped with FRP strips," *Composite Structures*, vol. 200, pp. 810–828, 2018.

[13] M. T. Jameel, M. N. Sheikh, and M. N. S. Hadi, "Behaviour of circularized and FRP wrapped hollow concrete specimens under axial compressive load," *Composite Structures*, vol. 171, pp. 538–548, 2017.

[14] Y. Li, M.-F. Xie, and J.-B. Liu, "Experimental study on the seismic behaviour of reinforced concrete bridge piers strengthened by BFRP sheets," *Advances in Civil Engineering*, vol. 2019, Article ID 4169421, 11 pages, 2019.

[15] A. Raza, Q. u. Z. Khan, and A. Ahmad, "Numerical investigation of load-carrying capacity of GFRP-reinforced rectangular concrete members using CDP model in ABAQUS," *Advances in Civil Engineering*, vol. 2019, Article ID 1745341, 21 pages, 2019.

[16] M. Fossetti, F. Basone, G. D'Arenzo, G. Macaluso, and A. F. Siciliano, "FRP-confined concrete columns: a new procedure for evaluating the performance of square and circular sections," *Advances in Civil Engineering*, vol. 2018, Article ID 2543850, 15 pages, 2018.

[17] C. Del Vecchio, M. Di Ludovico, A. Prota, and G. Manfredi, "Modelling beam-column joints and FRP strengthening in the seismic performance assessment of RC existing frames," *Composite Structures*, vol. 142, pp. 107–116, 2016.

[18] M. Lesani, M. R. Bahaari, and M. M. Shokrieh, "Numerical investigation of FRP-strengthened tubular T-joints under axial compressive loads," *Composite Structures*, vol. 100, pp. 71–78, 2013.

[19] E. Esmaeeli, F. Danesh, K. F. Tee, and S. Eshghi, "A combination of GFRP sheets and steel cage for seismic strengthening of shear-deficient corner RC beam-column joints," *Composite Structures*, vol. 159, no. Supplement C, pp. 206–219, 2017.

[20] S. S. Mahini and H. R. Ronagh, "Strength and ductility of FRP web-bonded RC beams for the assessment of retrofitted beam-column joints," *Composite Structures*, vol. 92, no. 6, pp. 1325–1332, 2010.

[21] A. Mukherjee and M. Joshi, "FRPC reinforced concrete beam-column joints under cyclic excitation," *Composite Structures*, vol. 70, no. 2, pp. 185–199, 2005.

[22] V. V. Cao and H. R. Ronagh, "Reducing the seismic damage of reinforced concrete frames using FRP confinement," *Composite Structures*, vol. 118, pp. 403–415, 2014.

[23] V. V. Cao and S. Q. Pham, "Comparison of CFRP and GFRP wraps on reducing seismic damage of deficient reinforced concrete structures," *International Journal of Civil Engineering*, vol. 17, no. 11, pp. 1667–1681, 2019.

[24] E. I. Saqan, H. A. Rasheed, and T. Alkhrdaji, "Evaluation of the seismic performance of reinforced concrete frames strengthened with CFRP fabric and NSM bars," *Composite Structures*, vol. 184, no. C, pp. 839–847, 2018.

[25] L. Lam and J. G. Teng, "Design-oriented stress-strain model for FRP-confined concrete," *Construction and Building Materials*, vol. 17, no. 6-7, pp. 471–489, 2003.

[26] Y.-Y. Wei and Y.-F. Wu, "Unified stress-strain model of concrete for FRP-confined columns," *Construction and Building Materials*, vol. 26, no. 1, pp. 381–392, 2012.

[27] M. Samaan, A. Mirmiran, and M. Shahawy, "Model of concrete confined by fiber composites," *Journal of Structural Engineering*, vol. 124, no. 9, pp. 1025–1031, 1998.

[28] C. Pellegrino and C. Modena, "Analytical model for FRP confinement of concrete columns with and without internal steel reinforcement," *Journal of Composites for Construction*, vol. 14, no. 6, pp. 693–705, 2010.

[29] S. A. Sheikh and G. Yau, "Seismic behavior of concrete columns confined with steel and fiber-reinforced polymers," *ACI Structural Journal*, vol. 99, no. 1, pp. 72–80, 2002.

[30] A. Rahai and H. Akbarpour, "Experimental investigation on rectangular RC columns strengthened with CFRP composites under axial load and biaxial bending," *Composite Structures*, vol. 108, pp. 538–546, 2014.

[31] M. H. Harajli and A. A. Rteil, "Effect of confinement using fiber-reinforced polymer or fiber-reinforced concrete on seismic performance of gravity load-designed columns," *ACI Structural Journal*, vol. 101, no. 1, pp. 47–56, 2004.

[32] M. K. Zaki, "Optimal performance of FRP strengthened concrete columns under combined axial-flexural loading," *Engineering Structures*, vol. 46, pp. 14–27, 2013.

[33] A. Fam and J.-K. Son, "Finite element modeling of hollow and concrete-filled fiber composite tubes in flexure: optimization of partial filling and a design method for poles," *Engineering Structures*, vol. 30, no. 10, pp. 2667–2676, 2008.

[34] R. Garcia, I. Hajirasouliha, and K. Pilakoutas, "Seismic behaviour of deficient RC frames strengthened with CFRP

composites," *Engineering Structures*, vol. 32, no. 10, pp. 3075–3085, 2010.
[35] A. Balsamo, A. Colombo, G. Manfredi, P. Negro, and A. Prota, "Seismic behavior of a full-scale RC frame repaired using CFRP laminates," *Engineering Structures*, vol. 27, no. 5, pp. 769–780, 2005.
[36] M. D. Ludovico, A. Prota, G. Manfredi, and E. Cosenza, "Seismic strengthening of an under-designed RC structure with FRP," *Earthquake Engineering & Structural Dynamics*, vol. 37, pp. 141–162, 2008.
[37] M. D. Ludovico, G. Manfredi, E. Mola, P. Negro, and A. Prota, "Seismic behavior of a full-scale RC structure retrofitted using GFRP laminates," *Journal of Structural Engineering*, vol. 134, no. 5, pp. 810–821, 2008.
[38] A. Mortezaei, H. R. Ronagh, and A. Kheyroddin, "Seismic evaluation of FRP strengthened RC buildings subjected to near-fault ground motions having fling step," *Composite Structures*, vol. 92, no. 5, pp. 1200–1211, 2010.
[39] H. Ozkaynak, E. Yuksel, O. Buyukozturk, C. Yalcin, and A. A. Dindar, "Quasi-static and pseudo-dynamic testing of infilled RC frames retrofitted with CFRP material," *Composites Part B: Engineering*, vol. 42, no. 2, pp. 238–263, 2011.
[40] G. E. Thermou, S. J. Pantazopoulou, and A. S. Elnashai, "Global interventions for seismic upgrading of substandard RC buildings," *Journal of Structural Engineering*, vol. 138, no. 3, pp. 387–401, 2012.
[41] X. K. Zou, J. G. Teng, L. De Lorenzis, and S. H. Xia, "Optimal performance-based design of FRP jackets for seismic retrofit of reinforced concrete frames," *Composites Part B: Engineering*, vol. 38, no. 5-6, pp. 584–597, 2007.
[42] S. W. Choi, Y. Kim, and H. S. Park, "Multi-objective seismic retrofit method for using FRP jackets in shear-critical reinforced concrete frames," *Composites Part B: Engineering*, vol. 56, pp. 207–216, 2014.
[43] The MathWorks I, (2014) MATLAB, Version R2014a.
[44] T. Takeda, M. A. Sozen, and N. N. Nielsen, "Reinforced concrete response to simulated earthquakes," *Journal of the Structural Division*, vol. 96, pp. 2557–2573, 1970.
[45] S. A. Sheikh and S. S. Khoury, "Confined concrete columns with stubs," *ACI Structural Journal*, vol. 90, no. 4, pp. 414–431, 1993.
[46] W. W. L. Chan, "The ultimate strength and deformation of plastic hinges in reinforced concrete frameworks," *Magazine of Concrete Research*, vol. 7, no. 21, pp. 121–132, 1955.
[47] A. L. L. Baker and A. M. N. Amarakone, "Inelastic hyperstatic frames analysis," in *Proceedings of the International Symposium on the Flexural Mechanics of Reinforced Concrete*, ASCE-ACI, Miami, FL, USA, pp. 85–142, October 1964.
[48] H. E. H. Roy and M. A. Sozen, "Ductility of concrete," in *Proceedings of the International Symposium on the Flexural Mechanics of Reinforced Concrete*, ASCE-ACI, Miami, FL, USA, pp. 213–224, October 1964.
[49] M. T. M. Soliman and C. W. Yu, "The flexural stress-strain relationship of concrete confined by rectangular transverse reinforcement," *Magazine of Concrete Research*, vol. 19, no. 61, pp. 223–238, 1967.
[50] M. Sargin, S. K. Ghosh, and V. K. Handa, "Effects of lateral reinforcement upon the strength and deformation properties of concrete," *Magazine of Concrete Research*, vol. 23, no. 75-76, pp. 99–110, 1971.
[51] D. C. Kent and R. Park, "Flexural members with confined concrete," *Journal of the Structural Division*, vol. 97, no. 7, pp. 1969–1990, 1971.
[52] R. Park, M. J. N. Priestley, and W. D. Gill, "Ductility of square-confined concrete columns," *Journal of the Structural Division*, vol. 108, pp. 929–950, 1982.
[53] V. V. Cao, H. R. Ronagh, M. Ashraf, and H. Baji, "A new damage index for reinforced concrete structures," *Earthquakes and Structures*, vol. 6, no. 6, pp. 581–609, 2014.
[54] L. Lam and J. G. Teng, "Design-Oriented stress-strain model for FRP-confined concrete in rectangular columns," *Journal of Reinforced Plastics and Composites*, vol. 22, no. 13, pp. 1149–1186, 2003.
[55] A. Eslami and H. R. Ronagh, "Effect of FRP wrapping in seismic performance of RC buildings with and without special detailing - a case study," *Composites Part B: Engineering*, vol. 45, no. 1, pp. 1265–1274, 2013.
[56] A. D. Luca, F. Nardone, F. Matta, A. Nanni, G. P. Lignola, and A. Prota, "Structural evaluation of full-scale FRP-confined reinforced concrete columns," *Journal of Composites for Construction*, vol. 15, no. 1, pp. 112–123, 2011.
[57] L.-M. Wang and Y.-F. Wu, "Effect of corner radius on the performance of CFRP-confined square concrete columns: Test," *Engineering Structures*, vol. 30, no. 2, pp. 493–505, 2008.
[58] M. H. Harajli, E. Hantouche, and K. Soudki, "Stress-strain model for Fiber-Reinforced Polymer jacketed concrete columns," *ACI Structural Journal*, vol. 103, no. 5, pp. 672–682, 2006.
[59] G. Wu, Z. S. Wu, and Z. T. Lü, "Design-oriented stress-strain model for concrete prisms confined with FRP composites," *Construction and Building Materials*, vol. 21, no. 5, pp. 1107–1121, 2007.
[60] M. N. Youssef, M. Q. Feng, and A. S. Mosallam, "Stress-strain model for concrete confined by FRP composites," *Composites Part B: Engineering*, vol. 38, no. 5-6, pp. 614–628, 2007.
[61] T. Ozbakkaloglu, J. C. Lim, and T. Vincent, "FRP-confined concrete in circular sections: review and assessment of stress-strain models," *Engineering Structures*, vol. 49, pp. 1068–1088, 2013.
[62] S. Rocca, N. Galati, and A. Nanni, "Review of design guidelines for FRP confinement of reinforced concrete columns of noncircular cross sections," *Journal of Composites for Construction*, vol. 12, no. 1, pp. 80–92, 2008.
[63] A. Mirmiran, M. Samaan, S. Cabrera, and M. Shahawy, "Design, manufacture and testing of a new hybrid column," *Construction and Building Materials*, vol. 12, no. 1, pp. 39–49, 1998.
[64] A. Mirmiran, M. Shahawy, M. Samaan, H. E. Echary, J. C. Mastrapa, and O. Pico, "Effect of column parameters on FRP-confined concrete," *Journal of Composites for Construction*, vol. 2, no. 4, pp. 175–185, 1998.
[65] M. N. Fardis and H. H. Khalili, "FRP-encased concrete as a structural material," *Magazine of Concrete Research*, vol. 34, no. 121, pp. 191–202, 1982.
[66] ACI (2008), Guide for the Design and Construction of Externally Bonded FRP Systems for Strengthening Concrete Structures (ACI 440.2R-08).
[67] S. Rocca, N. Galati, and A. Nanni, "Interaction diagram methodology for design of FRP-confined reinforced concrete columns," *Construction and Building Materials*, vol. 23, no. 4, pp. 1508–1520, 2009.
[68] R. Realfonzo and A. Napoli, "Confining concrete members with FRP systems: predictive vs design strain models," *Composite Structures*, vol. 104, pp. 304–319, 2013.
[69] H. Baji, H. R. Ronagh, and C. Q. Li, "Probabilistic design models for ultimate strength and strain of FRP-confined

concrete," *Journal of Composites for Construction*, vol. 20, no. 6, Article ID 04016051, 2016.
[70] H. Baji, "Calibration of the FRP resistance reduction factor for FRP-confined reinforced concrete building columns," *Journal of Composites for Construction*, vol. 21, no. 3, Article ID 04016107, 2017.
[71] T. Chaudat, C. Garnier, S. Cvejic, S. Poupin, M. Le Corre, and M. Mahe, *ECOLEADER Project no. 2: Seismic Tests On A Reinforced Concrete Bare Frame with FRP retrofitting-Tests Report*, CEA, Saclay, France, 2005.
[72] Computers and Structures Inc, (2017), SAP2000 Version 19.2.0.
[73] H. R. Ronagh and A. Eslami, "Flexural retrofitting of RC buildings using GFRP/CFRP - a comparative study," *Composites Part B: Engineering*, vol. 46, pp. 188–196, 2013, http://dx.doi.org/10.1016/j.compositesb.2012.09.072.
[74] ICBO, "Uniform building code," *International Conference of Building Officials*, ICBO, Whittier, CA, USA, 1994.
[75] J. M. Bracci, A. M. Reinhorn, and J. B. Mander, "Seismic resistance of reinforced concrete frame structures designed for gravity loads: performance of structural system," *ACI Structural Journal*, vol. 92, no. 5, pp. 597–608, 1995.
[76] J. M. Bracci, *Experimental and Analytical Study of Seismic Damage and Retrofit of Lightly Reinforced Concrete Structures in Low Seismicity Zones*, Ph.D. Thesis, State University of New York at Buffalo, New York, NY, USA, 1992.
[77] PEER, (2019), PEER Ground Motion Database. https://ngawest2.berkeley.edu/site.
[78] ACI, *Building Code Requirements for Structural Concrete (ACI 318M-08) and Commentary*, American Concrete Institute, Farmington Hills, MI, USA, 2008.
[79] ASCE, *Prestandard and Commentary for the Seismic Rehabilitation of Buildings*, Federal Emergency Management Agency, Washington, DC, USA, 2000.
[80] ASCE, *Minimum Design Loads for Buildings and Other Structures*, American Society of Civil Engineers, Farmington Hills, MI, USA, 2010.